





# Synergistic Antibacterial Potential of Greenly Synthesized Silver Nanoparticles with Fosfomycin Against Some Nosocomial Bacterial Pathogens

Mohammed Mubarak Aljeldah <sup>1</sup>, Mohamed Taha Yassin <sup>2</sup>, Ashraf Abdel-Fattah Mostafa <sup>2</sup>,  
Mourad AM Aboul-Soud <sup>3</sup>

<sup>1</sup>Department of Clinical Laboratory Sciences, College of Applied Medical Sciences, University of Hafr Al Batin, Hafr Al-Batin, Saudi Arabia; <sup>2</sup>Botany and Microbiology Department, College of Science, King Saud University, Riyadh, Saudi Arabia; <sup>3</sup>Chair of Medical and Molecular Genetics Research, Department of Clinical Laboratory Sciences, College of Applied Medical Sciences, King Saud University, Riyadh, Saudi Arabia

Correspondence: Mohammed Mubarak Aljeldah, College of Applied Medical Sciences, University of Hafr Al Batin, Email mmaljeldah@uhb.edu.sa, Mourad AM Aboul-Soud, Chair of Medical and Molecular Genetics Research, College of Applied Medical Sciences, King Saud University, Email Maboulsoud@ksu.edu.sa

**Introduction:** A considerable number of morbidities and fatalities occur worldwide as a result of the multidrug resistant microorganisms that cause a high prevalence of nosocomial bacterial infections. Hence, the current investigation was conducted to evaluate the antibacterial potency of green fabricated silver nanoparticles (AgNPs) against four different nosocomial pathogens.

**Methods:** The flower extract of *Hibiscus sabdariffa* mediated green fabrication of AgNPs and their physicochemical features were scrutinized using different techniques. Antimicrobial activity of the biogenic AgNPs and their synergistic patterns with fosfomycin antibiotic were evaluated using disk diffusion assay.

**Results and Discussion:** UV spectral analysis affirmed the successful formation of AgNPs through the detection of broad absorption band at 395 and 524 nm, indicating the surface plasmon resonance of the biofabricated AgNPs. In this setting, the biofabricated AgNPs demonstrated average particle size of 58.682 nm according to transmission electron microscope (TEM) micrographs. The detected hydrodynamic diameter was higher than that noticed by TEM analysis, recording 72.30 nm in diameter and this could be attributed to the action of capping agents, which was confirmed by Fourier Transform Infrared (FT-IR) analysis. Disk diffusion assay indicated the antibacterial potency of biogenic AgNPs (50 µg/disk) against *Enterobacter cloacae*, Methicillin-resistant *Staphylococcus aureus*, *Klebsiella pneumoniae* and *Escherichia coli* strains with relative inhibition zone diameters of  $12.82 \pm 0.36$  mm,  $14.54 \pm 0.15$  mm,  $18.35 \pm 0.24$  mm and  $21.69 \pm 0.12$  mm, respectively. In addition, *E. coli* was found to be the most susceptible strain to the biogenic AgNPs. However, the highest synergistic pattern of AgNPs-fosfomycin combination was detected against *K. pneumoniae* strain recording relative synergistic percentage of 64.22%. In conclusion, the detected synergistic efficiency of AgNPs and the antibiotic fosfomycin highlight the potential for utilizing this combination in the biofabrication of effective antibacterial agents against nosocomial pathogens.

**Keywords:** green synthesis, *Hibiscus sabdariffa*, silver nanoparticles, resistance, synergism, fosfomycin

## Introduction

Antimicrobial resistance is one of the main intimidations to human health, which leads to higher rates of morbidity and mortality from hospital and community-acquired infections caused by multidrug resistance bacterial pathogens.<sup>1</sup> Strikingly, the US Centers for Disease Control and Prevention (CDC) estimate that the direct healthcare cost in the US has increased by 20 billion dollars as a result of antibiotic resistance.<sup>2</sup> The high prevalence of multidrug resistant bacterial strains calls for the development of innovative antibacterial agents to effectively control nosocomial infections in hospitals and other healthcare settings.<sup>3</sup> Recent advances in nanotechnology have led to the fabrication of nano-scale particles with strong antibacterial properties against multidrug resistant bacterial pathogens.<sup>4</sup> Due to their distinctive characteristics and diverse range of uses, silver nanoparticles (AgNPs) have attracted a lot of attention from researchers working across several fields in recent years.<sup>5</sup>

The majority of chemical procedures for nanoparticles synthesis are excessively expensive and employ hazardous chemicals that pose a number of concerns to the environment.<sup>6</sup> On the other hand, the biosynthetic pathway uses plants and microbes to synthesize nanoparticles that are safe, biocompatible, and environmentally benign for use in biomedical applications.<sup>7</sup> In fact, using plant materials can be easier and more advantageous for fabricating nanosilver than using microbes or chemicals because there is no risk of bacterial or toxic chemical contamination, and using less energy.<sup>8</sup> It has been demonstrated that Roselle (*Hibiscus sabdariffa* L.) possesses a number of bioactivities with medicinal advantages.<sup>9</sup> In this context, numerous reports on *H. sabdariffa* L. have demonstrated that the plant has a potential role on reducing the risk of hyperlipidemia, hyperglycemia, diabetes mellitus, hypertension, cancer, obesity and inflammation.<sup>10</sup> Furthermore, *H. sabdariffa* extracts were primarily consists of the phenolic constituents as polyphenolic acid, anthocyanins, flavonoids, ascorbic acid, malic acid, hydroxyl benzoic acid, etc.<sup>11</sup> Accordingly, it is possible to synthesize AgNPs utilizing *H. sabdariffa* extracts as a reductant and stabilizer since phenols are important in the reduction of metal ions.<sup>12</sup> Recent study was achieved to investigate the antibacterial activities of AgNPs synthesized utilizing aqueous plant extracts of *Berberis vulgaris*, *Brassica nigra*, *Capsella bursa-pastoris*, *Lavandula angustifolia* and *Origanum vulgare*, demonstrating that AgNPs of *B. nigra* and *L. angustifolia* extracts exhibited the most effective antimicrobial potency against *Staphylococcus aureus* CCM 4223, and *Escherichia coli* CCM 3988 strains compared to the other biosynthesized AgNPs.<sup>13</sup> In addition, *Citrus limon* zest extract mediated green bioformulation of AgNPs which were found to display potent antimicrobial activity against *E. coli*, and *S. aureus* strains.<sup>14</sup> The widespread incidence of drug resistance bacterial strains demands the bioformulation of novel and effective antibacterial combinations.<sup>15</sup> In this setting, previous report demonstrated the green biofabrication of AgNPs utilizing *Polygonatum graminifolium* leaf extract, detecting the highest synergistic activity with rifampicin antibiotic compared to kanamycin and ampicillin antibiotics.<sup>16</sup> Accordingly, there is an increasing necessity to investigate new synergistic patterns of other AgNPs-antibiotic combinations to overcome the widespread incidence of drug resistance strains. A prior study examined the antibacterial effectiveness of AgNPs produced from *Ocimum basilicum* L. and *H. sabdariffa* L. leaf extracts against *Salmonella enterica* (add ref).<sup>17</sup> However, another report evaluated only the cytotoxic activity of AgNPs generated using *H. sabdariffa* leaf extract and did not investigate the antibacterial activity of the synthesized AgNPs.<sup>18</sup> As a result, the current study was carried out to determine the antibacterial activity of green AgNPs synthesized using *H. sabdariffa* flower extract against four nosocomial bacterial pathogens, namely methicillin-resistant *Staphylococcus aureus* (MRSA), *E. coli*, *K. pneumonia*, and *E. cloacae* strains, as well as the relative synergism between the biogenic AgNPs and fosfomycin antibiotic for the first time.

## Materials and Methods

### Preparation of Flower Water Extract of *H. sabdariffa*

In Riyadh, Saudi Arabia, dried flowers of *H. sabdariffa* were bought from a local market. The herbarium at the Botany and Microbiology department verified the identification of the acquired plant materials. *Hibiscus* dried flowers were washed once with tap water followed by rinsing them with distilled H<sub>2</sub>O for three times in a row and finally left for complete dryness. To obtain a fine and uniform powder, the dried flowers of *H. sabdariffa* were crushed using a mechanical blender. Fifty grams of the dried flower powder were submerged in 500 mL flask comprising 200 mL distilled H<sub>2</sub>O and left for half an hour over hot plate (60°C). Afterwards, the mixture was stirred over a magnetic stirrer for 24 hr at 25°C and finally the mixture was clarified using Whatman filter paper grade 1 to get rid of any impurities and gain a clear filtrate. Finally, the extracts were stored for future use in refrigerator at 4°C.<sup>19</sup>

### Biofabrication of AgNPs

Firstly, 10 mL of the flower water extract of *H. sabdariffa* was added to 90 mL of 1mM of the colorless AgNO<sub>3</sub> (Sigma-Aldrich, Missouri, USA) solution. Afterwards, the reduction procedure was successfully achieved by dropwise addition of 1 M NaOH for the adjustment of the pH value of reaction mixture to 6.9 then the reaction mixture was incubated at room temperature under dark conditions. The green biofabrication of the AgNPs was monitored visually by a color shift from red to dark brown color. The biofabricated AgNPs were collected from the bioreduced mixture by centrifugation at

10,000 rpm for 10 minutes. The recovered AgNPs were then washed three times with deionized water to remove impurities and finally dried at 80°C in an oven for later physicochemical assessment.<sup>20</sup>

## Characterization of Biofabricated AgNPs

Utilizing a variety of techniques, the physicochemical characteristics of biofabricated AgNPs were examined. After dispersing the biogenic AgNPs in distilled H<sub>2</sub>O, the absorbance was measured in the wavelength range of 200–800 nm using a UV-VIS-NIR spectrophotometer (UV-1601, Shimadzu, Japan), with distilled H<sub>2</sub>O serving as a blank. The TEM analysis was performed utilizing a Transmission Electron Microscope (JEOL, JEM1011, Tokyo, Japan) to detect the morphological characteristics and size distribution pattern of the biogenic AgNPs by producing high-resolution two-dimensional images at a voltage of 100 kV. In this context, the biogenic AgNPs were rinsed three times with deionized water then 5 µL of the sonicated AgNPs solution were dropped over a carbon-coated copper grid, and finally allowed to dry at room temperature for 48 h. Fourier Transform Infrared (FT-IR) Spectroscopy (Shimadzu, Kyoto, IR Affinity 1, Japan) was conducted to do a spectral study of the biofabricated AgNPs in order to identify the key functional groups responsible for reduction, stabilization, and capping of silver nanomaterials. In addition, the elemental pattern of the biofabricated AgNPs was detected utilizing Energy Dispersive X-ray (EDX) analyzer (JEOL, JSM-6380 LA, Tokyo, Japan). Moreover, the X-ray powder diffraction (XRD) was achieved by diffractometer (SHIMADZU-XRD 6000) using a Cu K $\alpha$  radiation ( $\lambda=1.5406\text{\AA}$ ) to investigate crystallographic nature of AgNPs whereas the hydrodynamic particle size and net surface charge were investigated using a zeta sizer instrument (Malvern Instruments Ltd.; zs90, Worcestershire, UK).<sup>21</sup>

## Antibacterial Screening of Biofabricated AgNPs

Four nosocomial bacterial strains, including Methicillin-resistant *Staphylococcus aureus* (ATCC 43300), *Escherichia coli* (ATCC 25922), *Klebsiella pneumoniae* (ATCC 700603), and *Enterobacter cloacae* (ATCC 13047), were utilized to investigate the biofabricated AgNPs for their antibacterial efficacy. The antibacterial bioactivity of the eco-friendly prepared AgNPs against the targeted bacterial pathogens was investigated using the standard disk diffusion assay as described in prior study.<sup>22</sup> Briefly, microbial suspensions of different bacterial isolates were prepared by immersing freshly prepared bacterial inoculums into 0.85% sterile saline solution then adjusted utilizing 0.5 McFarland standard to accomplish viable bacterial cell count of  $1.0 \times 10^8$  cfu/mL. Freshly prepared Mueller–Hinton agar (MHA) plates were then seeded with 0.5 mL of the microbial suspension. The dried AgNPs were then dissolved in methanol. 8 mm diameter sterile filter paper disks were impregnated with 50 and 100 µg of the dissolved AgNPs,<sup>23</sup> with the methanol solvent-only disks serving as the negative controls. Conversely, fosfomycin disks (50 µg) plus 50 µg glucose-6-phosphate were used as positive controls. In this regard, the standard fosfomycin disodium salt hydrate was purchased from Sigma-Aldrich, USA and stock solution of fosfomycin antibiotic was prepared for subsequent use. The stock solution was prepared by dissolving of 409.6 mg of fosfomycin salt in 40 mL of distilled water to attain a final fosfomycin concentration of 10.24 mg/mL.<sup>34</sup> The impregnated disks were placed over the inoculated MHA plates and the plates were then incubated at 37 °C for 24 h followed by measuring the zone of inhibitions using Vernier caliper. Disc diffusion test was done in triplicates, and the inhibitory zones were measured and presented as a mean of triplicates  $\pm$  standard error. The minimum inhibitory concentration (MIC) of the biofabricated AgNPs was investigated against *E. coli* strain which revealed the highest susceptibility to the biogenic AgNPs. Broth microdilution assay was conducted to detect MIC of the bioformulated AgNPs utilizing 96-well microtiter plates as reported in previous reports.<sup>24</sup> The tested concentrations of AgNPs for MIC and MBC detection were (5, 10, 15, 20, 25, 30, 35 and 40 µg/mL). As the MIC concentration of AgNPs was detected to be 15µg/mL, the bactericidal concentration of the bio-prepared AgNPs was investigated by streaking from MIC wells of AgNPs concentrations (20, 25 and 30 µg/mL) onto freshly prepared MHA plates followed by incubation at 37 °C for 24 h and the lowest AgNPs concentration which showed no bacterial growth was registered as minimum bactericidal concentration (MBC).

## Evaluation of Fosfomycin-AgNPs Synergistic Patterns

The synergistic effectiveness of fosfomycin-AgNPs combination against the targeted nosocomial bacterial pathogens was investigated using the standard disk diffusion method.<sup>38</sup> Fresh MHA plates were prepared and inoculated with 0.5 mL of

the previously prepared bacterial suspension. Filter paper disks (8 mm in diameter) were filled with AgNPs (15 µg/disk) while another group of disks were filled with both of fosfomycin (50 µg) plus 50 µg glucose-6-phosphate and AgNPs (15 µg/disk) to investigate their combined synergistic action. Positive control disks were loaded with fosfomycin (50 µg) plus 50 µg glucose-6-phosphate whereas negative control ones were filter paper disks loaded with methanol solvent. The loaded disks were left for dryness then placed over the seeded MHA plates and finally the plates were incubated at 37 °C for 24 h. The synergistic potency percentage (%) was estimated according to the following formula:

Synergistic percentage =  $\frac{B-A}{A} \times 100$ , where A is the zone of inhibition of fosfomycin antibiotic and B is the zone of inhibition of fosfomycin-AgNPs combination.<sup>25</sup>

## Statistical Analysis

The study's experiments were all carried out in triplicates, and the data were analyzed using GraphPad Prism 8.0 (GraphPad Software, Inc., La Jolla, CA, USA).

## Results and Discussion

### Green Bioformulation of AgNPs

Green biofabrication of silver nanoparticles was achieved utilizing the water extract of *H. sabdariffa* extract as seen in Figure 1. The reduction process revealed the change of the colorless AgNO<sub>3</sub> solution to dark brown color after the addition of the flower water extract of *H. sabdariffa* (Figure 2). The observed broad peak absorbance, may have been caused by variations in particle size, which was further validated using the dynamic light scattering technique.<sup>26</sup> The dark brown color formation was reported to be owing to the excitation of the surface plasmon resonance (SPR), which is a distinctive feature of AgNPs. By the way, the absorption bands noticed at 395 and 524 nm could be ascribed to the surface plasmon resonance of the biogenic AgNPs (Figure 3).<sup>27</sup> The robust UV absorption peak seen at around 242 nm specified the existence of several organic constituents of the used plant extract which were recognized to interact with Ag<sup>+</sup> ions.<sup>28</sup> UV spectral data showed the formation of absorption peak with a shoulder at 395 nm and tail at longer wavelengths, indicating the bioformulation of polydispersed AgNPs. Our findings were in agreement with that of a prior report which indicated the SPR of AgNPs formulated using aqueous flower extract of *H. sabdariffa*, demonstrating

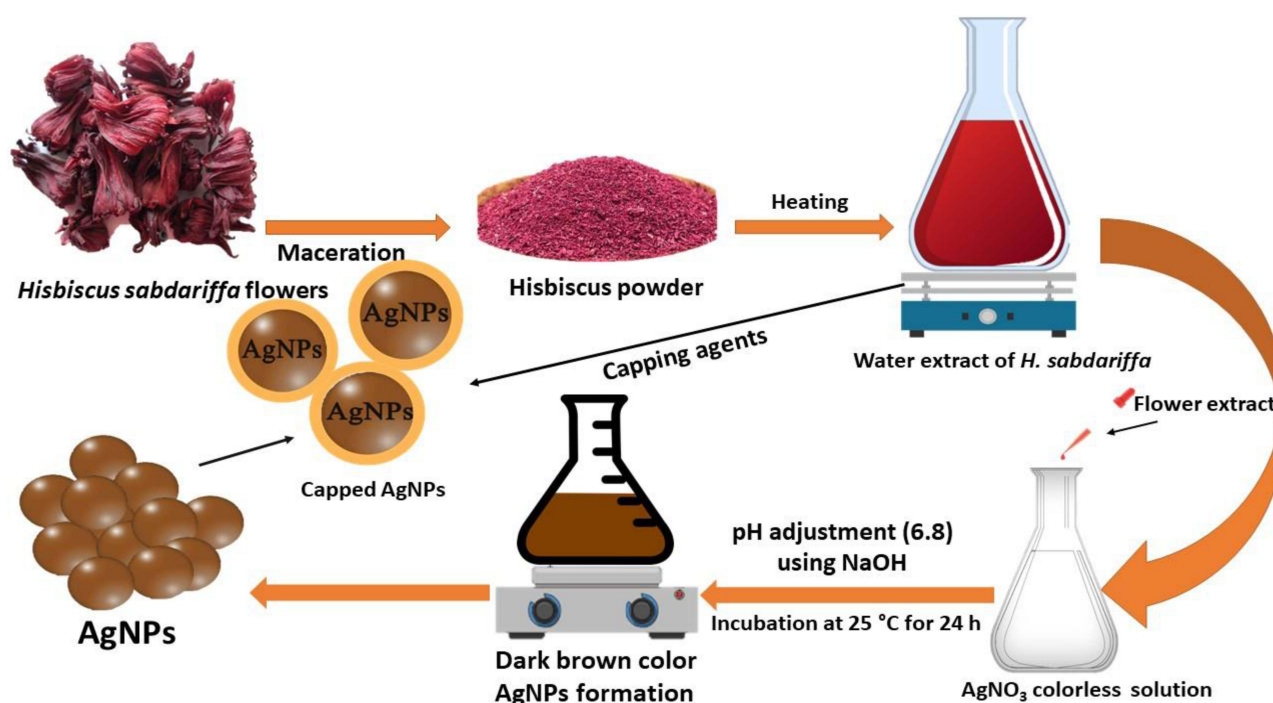


**Figure 1** Green biosynthesis of AgNPs utilizing flower water extract of *H. sabdariffa*.





**Figure 2** Green biosynthesis of nanosilver utilizing flower water extract of *H. sabdariffa*. (A) colorless  $\text{AgNO}_3$ , (B) flower extract of *H. sabdariffa*, (C) dark brown solution of silver nanoparticles.

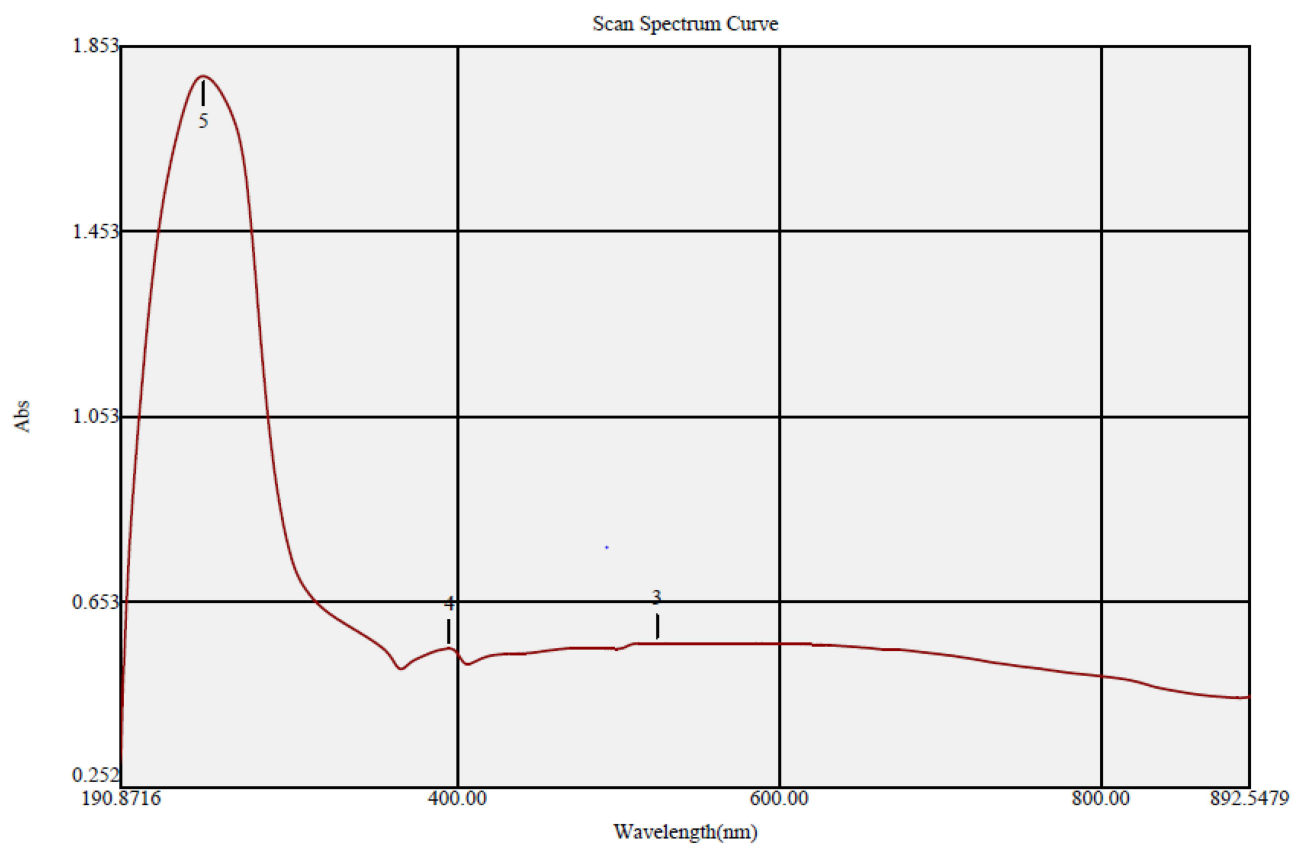


**Figure 3** UV spectrum of the biogenic AgNPs formulated utilizing *H. sabdariffa* flower extract (peak 3: 524 nm, peak 4: 395 nm, peak 5: 242 nm).

absorption peak at 399 nm.<sup>29</sup> The UV spectra exhibited a broad peak at 524 nm due to the activity of capping agents from the plant extract utilized in the synthesis technique, which adhered to the surface of the nanoparticles and provided a core shell-like structure. The presence of various functional groups such as phenols, alcohols, flavonoids, and amides serving as capping agents of the biogenic AgNPs was confirmed by FTIR analysis. Our findings were consistent with those of Shivaji et al, 2011, who observed the formation of a broad peak at 524 nm due to the action of these capping agents.<sup>30</sup> Another investigation further affirmed that the observed SPR band at 524 nm might be attributed to the formation of AgNPs aggregates with increasing the reaction time of AgNPs synthesis.<sup>31</sup>

## Transmission Electron Microscope (TEM) Analysis

Transmission electron microscopy (TEM) analysis was achieved to estimate the shape, size, surface morphology and topology of the biogenic AgNPs. According to Figure 4, the bulk of biofabricated AgNPs fall within the 20–100 nm size range. Additionally, the biogenic AgNPs had a polydispersed nature and a spherical form. Particle size distribution histogram revealed that average particle size of the biogenic AgNPs was  $58.682 \pm 1.96$  nm (Figure 5). Our results were in agreement with that of a previous study which demonstrated the green biosynthesis of AgNPs utilizing *Streptomyces atrovirens*, recording average particle size of 58 nm.<sup>32</sup> Another investigation reported the bioformulation of green AgNPs using water root extract of *Rumex hastatus*, demonstrating average particle size of 58 nm.<sup>33</sup>

## Elemental Mapping of the Biogenic AgNPs

Energy-dispersive X-ray (EDX) spectroscopy of the biosynthesized AgNPs indicated the presence of the following elements: silver, chloride, carbon, oxygen and silicon, with respective mass percentages of 74.01, 19.87, 3.01, 2.73 and

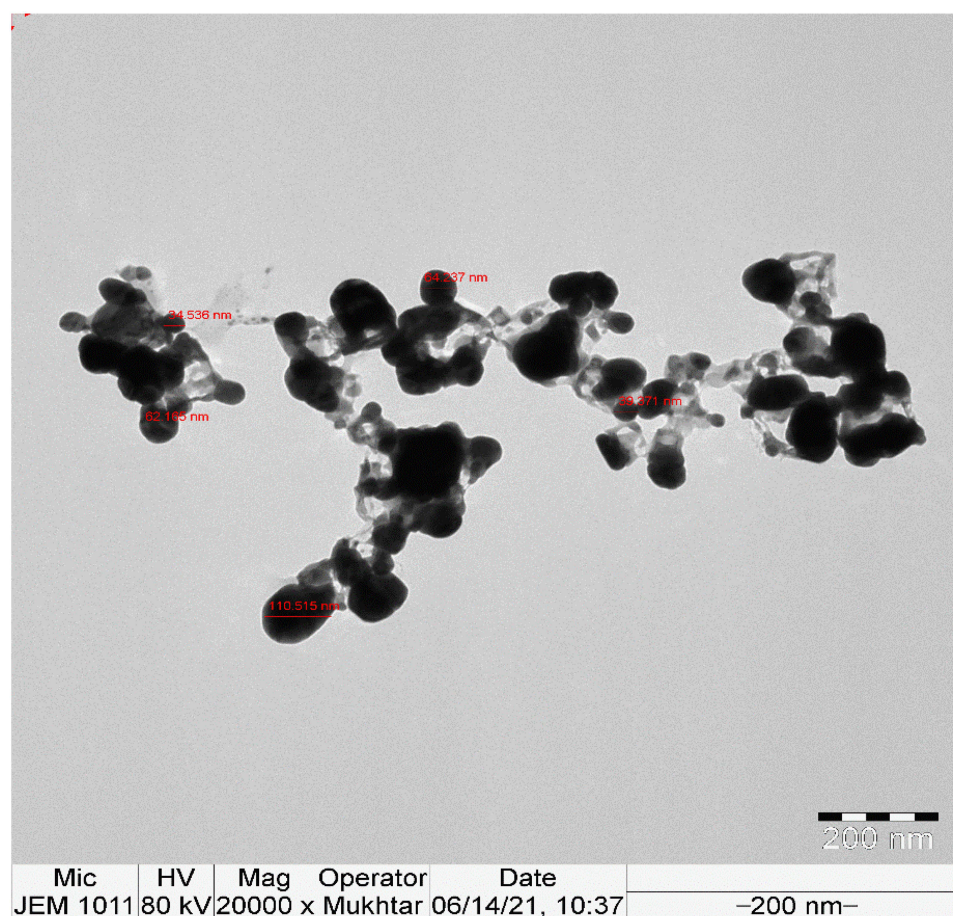


**Figure 4** TEM micrograph of the biofabricated AgNPs.

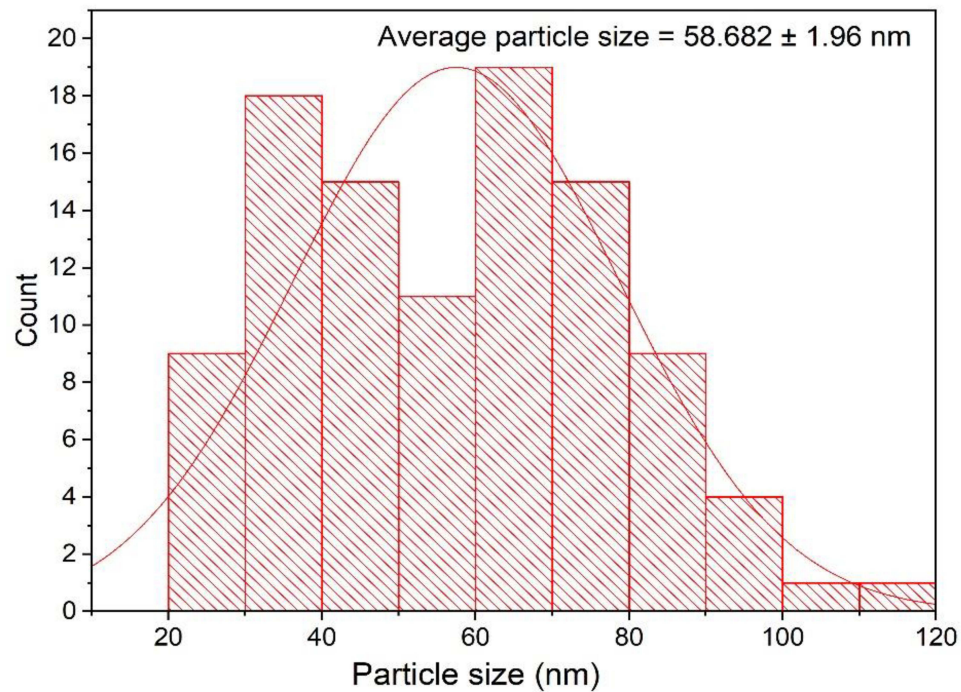


**Figure 5** Particle size distribution histogram of the biogenic AgNPs (number of analyzed particles was 102).

### *JED-2200 Series*

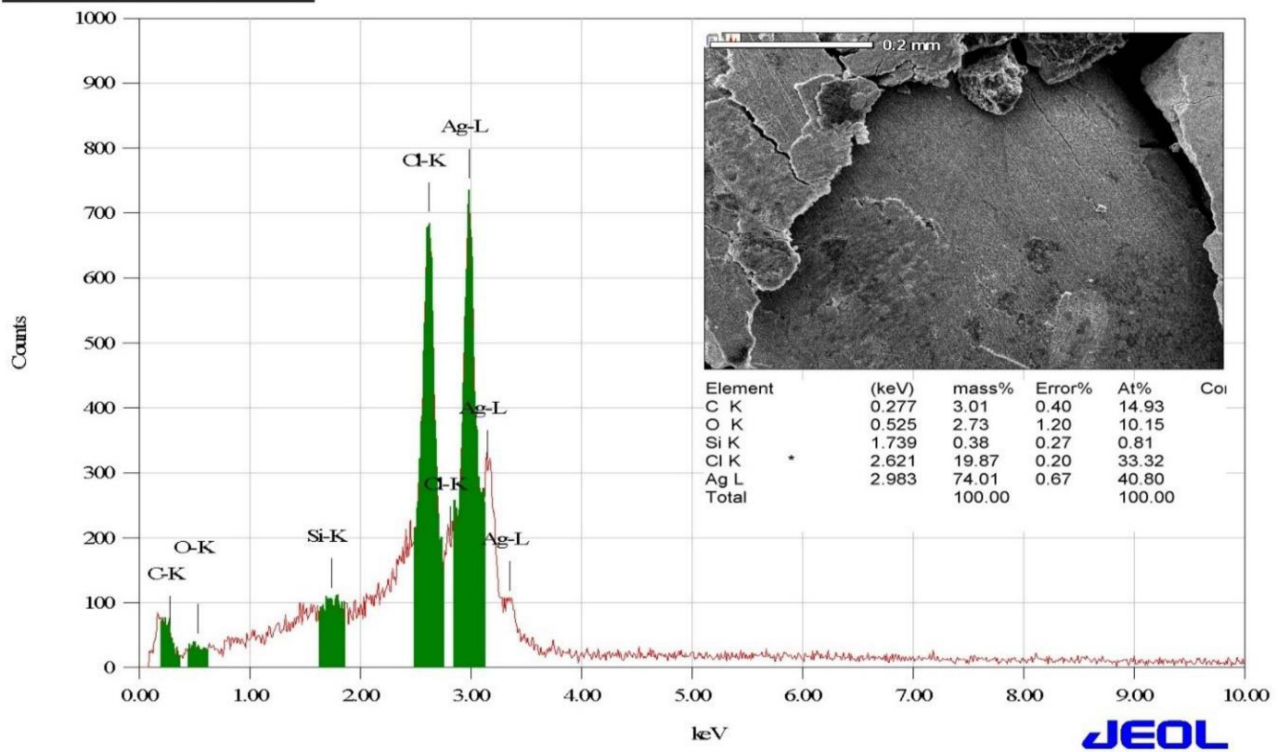


**Figure 6** EDX spectrum of the biosynthesized silver nanomaterials.

0.38%, respectively. In this regard, silver atoms were responsible for the strong signals at 2.983 keV, whereas silicon atoms were accountable for the weak signal at 1.739 keV (Figure 6). The high silver content detected by EDX analysis demonstrated the high efficacy of the green route of synthesizing silver nanoparticles using water extract of *H. sabdariffa*. On the other hand, the other signals observed at 2.621, 0.525 and 0.277 keV were assigned to the presence of chloride, oxygen and carbon atoms, respectively. In this regard, the noticed carbon traces could be assigned to the usage of conductive carbon tape through sample processing.<sup>34</sup> Moreover, the X-ray emission from the enzymes and proteins present in the aqueous extract of *H. sabdariffa* flowers resulted in the detection of other elements as silicon, chlorine, carbon, and oxygen.<sup>35</sup> In addition, the abundance of chloride ( $\text{Cl}^-$ ) ions in plants, which were found to be responsible for maintaining homeostasis and playing a crucial role during photosynthesis, was signified by other researchers as the reason for the strong peak of  $\text{Cl}^-$  detected by EDX spectrum of the biogenic AgNPs.<sup>36</sup> Communally, the odd elements as Si, and Cl apprehended by EDX elemental configuration were reported to be crucial for the bioreduction of  $\text{Ag}^+$  ions to synthesize elemental silver ( $\text{Ag}^0$ ), as well as for capping and stabilizing the biosynthesized AgNPs.<sup>37</sup>

### FTIR Analysis of the Biogenic Silver Nanoparticles

FTIR analysis of the biogenic AgNPs indicated the presence of eight absorbing bands at 3430.20, 2919.66, 2846.89, 1630.51, 1381.66, 1034.77, 760.69 and 539.29  $\text{cm}^{-1}$  as seen in Figure 7. The strong absorption band observed at 3430.20  $\text{cm}^{-1}$  revealed the O–H stretching of phenolic and flavonoid compounds capped on the biosynthesized AgNPs. However, C–H stretching of alkanes was observed due to the peaks detected at 2919.66 and 2846.89  $\text{cm}^{-1}$ . In addition, the intense absorption band detected at 1630.51  $\text{cm}^{-1}$  indicated the capping action of amides on the biosynthesized AgNPs whereas the weak band noticed at 1381.66  $\text{cm}^{-1}$  could be assigned to C–H bending of aldehydes (Table 1). Accordingly, this amide band indicated the possible association between  $\text{Ag}^+$  and proteins through free amino or carbonyl groups. The spectral data signified the presence of intense band at 1034.77  $\text{cm}^{-1}$  which could be assigned to C–O vibrations of alcohols. The detected C–O band of the biosynthesized AgNPs could be attributed to the capping action of *H. sabdariffa* secondary metabolites as demonstrated in a prior investigation.<sup>38</sup> On the other hand, the weak band

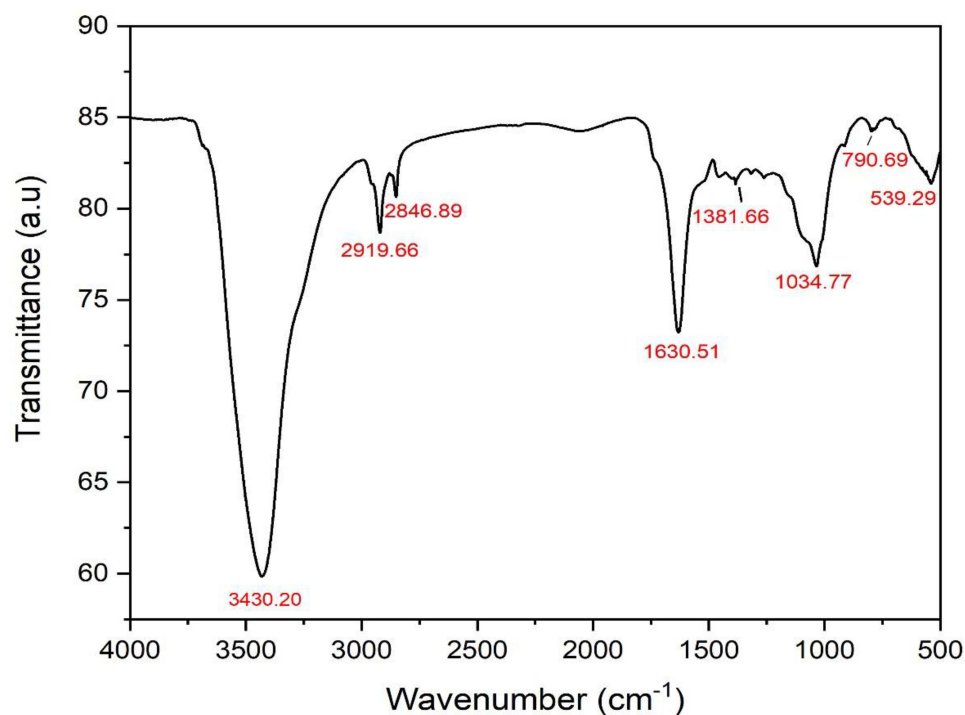


Figure 7 IR spectrum of the biosynthesized AgNPs.



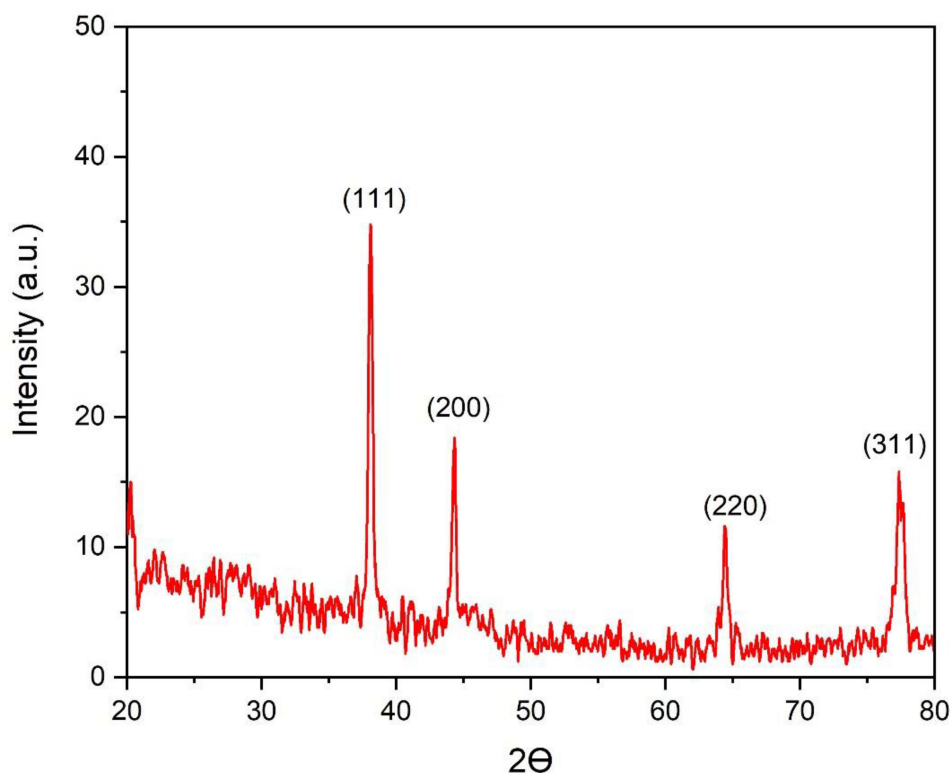
**Table I** Functional Groups of the Biosynthesized AgNPs

No.	Absorption Peak (cm <sup>-1</sup> )	Appearance	Functional Groups	Molecular Motion
1	3430.20	Strong, broad	Phenolics and flavonoids	O-H stretching
2	2919.66	Medium	Alkanes	C-H stretching
3	2846.89	Weak	Alkanes	C-H stretching
4	1630.51	Medium	Amides	C=O stretching
5	1381.66	Weak	Aldehydes	C-H bending
6	1034.77	Medium	Alcohols	C-O stretching
7	760.69	Weak	Aromatic compounds	C-H bending
8	539.29	Weak, broad	Alkyl halides	C-Cl stretching

observed at 760.69 cm<sup>-1</sup> could be assigned to the C-H bending of aromatic compounds whereas the minor band at 539.29 cm<sup>-1</sup> revealed the molecular vibrations of alkyl halide compound. Collectively, the observed functional groups as alcohols, flavonoids, amides, and aldehydes act as capping agents of the biosynthesized AgNPs, acting as electron shuttle by donating electrons to silver ions resulting in the successful formation of silver nanoparticles.<sup>39</sup>

### XRD Analysis of the Biogenic AgNPs

The crystalline phase and orientation of the biogenic AgNPs were detected utilizing X-ray powder diffraction (XRD) method. Four Bragg peaks at 2 theta (Θ) angles of 38, 44, 64, and 77° were detected by XRD diffractogram; these peaks correspond to (111), (200), (220), and (311) miller indices, affirming the synthesis of face-centered cubic (FCC) crystalline elemental silver, indexed with the JCPDS data 04–0783, indexed with the JCPDS data 04–0783 as seen in Figure 8.<sup>40</sup> Our results were in consistence with those of a prior investigation which demonstrated the green bioformulation of AgNPs utilizing water extract of *Pistacia atlantica* seeds, revealing Bragg peaks at 2Θ angles of 38°, 44°, 64° and 77°, which confirmed the cubic crystalline structure of the biosynthesized AgNPs.<sup>41</sup>

**Figure 8** XRD spectrum of the biosynthesized AgNPs.

Zeta Analysis of the Bioformulated AgNPs

Dynamic light scattering technique was achieved to detect the polydispersity index (PDI), size distribution and average hydrodynamic diameter of the biofabricated AgNPs. The International Organization for Standardization (ISO) determined that monodisperse samples are more likely to have polydispersity index (PDI) value lower than 0.05, whereas samples with a wide distribution of particle sizes are more likely to have  $PDI > 0.7$  (eg, polydisperse).<sup>42</sup> Accordingly, the estimated PDI value of the biogenic AgNPs was found to be 0.519 (Figure 9), indicating that the synthesized particles were moderately polydispersed. The green-synthesized AgNPs had an average hydrodynamic size of 72.03 nm, which was larger than the size of AgNPs noticed using TEM analysis (58.862 nm). This difference could be attributed to the action of the capping agents of *H. sabdariffa* flower extract, which result in increasing the hydrodynamic diameter of the synthesized particles. In this regard, the FTIR analysis supported the findings of the DLS technique, which examined the physical size of AgNPs as well as the capping agents.

Zeta potential analysis of the biogenic AgNPs is an indication of their stability in aqueous solutions. The detected zeta potential value of the biosynthesized AgNPs was found to be as  $-23.4$  mV as seen in Figure 10. Together, the biogenic AgNPs' high negative charge revealed that these nanoparticles were negatively charged all over their surface in aqueous solutions, highlighting their high colloidal dispersivity and long-term stability.<sup>43</sup> The presence of bioactive compounds in *H. sabdariffa* flower extract, which was demonstrated by FTIR analysis, may be the cause of the noticed negative charge of the biogenic AgNPs, confirming their ability to repel each other, and highlighting their stability and uniform distribution condition in water.<sup>44</sup>

Screening of the Antibacterial Potency of the Biosynthesized AgNPs

The bioactivity of the green AgNPs was assessed against four different bacterial strains using the standardized disk diffusion technique. In this regard, the produced AgNPs were screened at two concentrations (50 and 100  $\mu\text{g}/\text{disk}$ ) for

Results

	Size (d.nm):	% Intensity:	St Dev (d.n...
<b>Z-Average (d.nm):</b> 72.30	<b>Peak 1:</b> 119.9	93.6	83.75
<b>Pdl:</b> 0.519	<b>Peak 2:</b> 4254	5.0	986.9
<b>Intercept:</b> 0.779	<b>Peak 3:</b> 6.039	1.4	1.095
<b>Result quality :</b> Good			

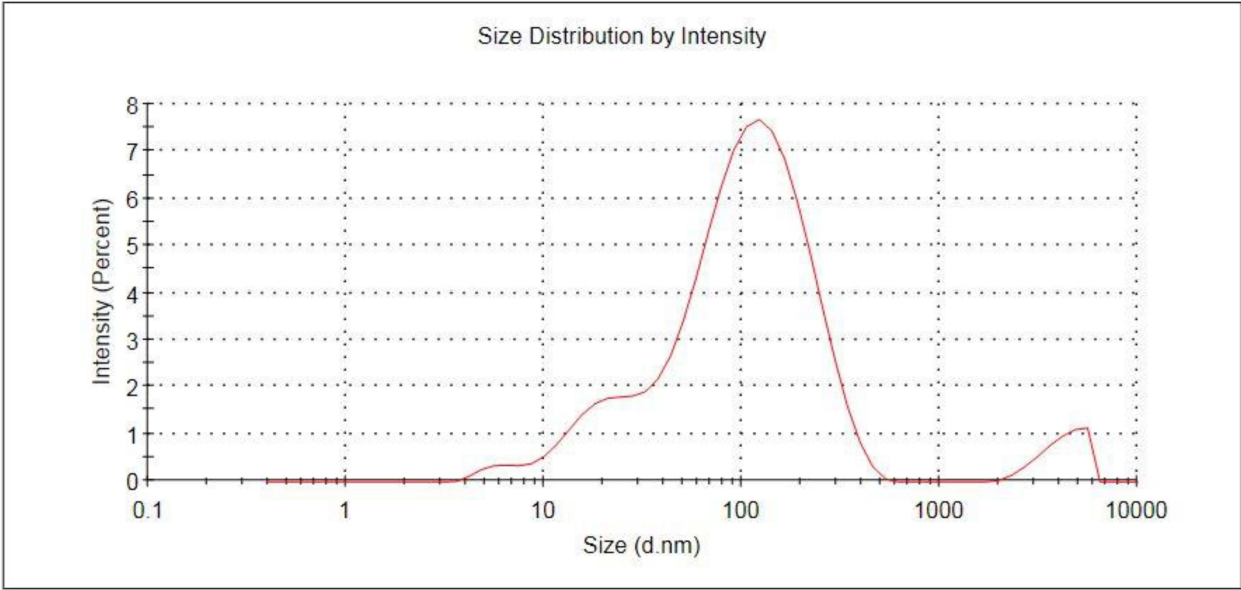
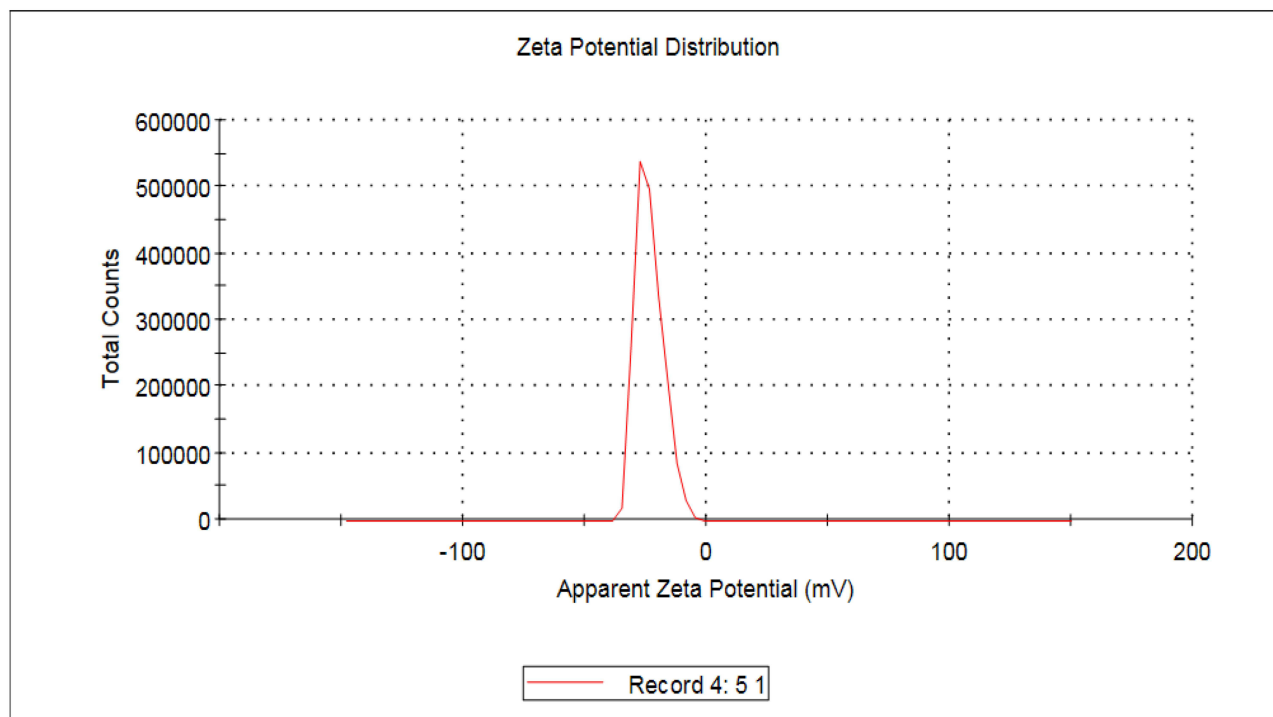


Figure 9 Size distribution pattern of the biogenic AgNPs using DLS technique.

## Results

	Mean (mV)	Area (%)	St Dev (mV)
<b>Zeta Potential (mV): -23.4</b>	<b>Peak 1: -23.4</b>	100.0	5.56
<b>Zeta Deviation (mV): 5.56</b>	<b>Peak 2: 0.00</b>	0.0	0.00
<b>Conductivity (mS/cm): 0.631</b>	<b>Peak 3: 0.00</b>	0.0	0.00
<b>Result quality : Good</b>			



**Figure 10** Zeta potential analysis of the biogenic AgNPs.

their antibacterial effectiveness against various bacterial strains, whereas fosfomycin antibiotic at a concentration of 50 µg/disk was utilized as positive control. The bioactivity of AgNPs was tested against nosocomial pathogens namely, *E. coli*, MRSA, *E. cloacae* and *A. baumannii*. *E. coli* is an evolving nosocomial bacterial pathogen causing issues in healthcare facilities.<sup>45</sup> Numerous illnesses, including UTI, septicemia, pneumonia, newborn meningitis, peritonitis, and gastroenteritis, are brought on by *E. coli*.<sup>46</sup> In this context, *E. coli* strain ATCC 25922 revealed the highest susceptibility to both concentrations of the biosynthesized AgNPs, recording inhibitory zones of  $21.69 \pm 0.12$  and  $23.18 \pm 0.36$  mm in diameter, respectively. These findings were higher than those reported in a previous report which indicated the green bioformulation of AgNPs utilizing water and ethanolic extracts of *Andrographis paniculata* stem, demonstrating inhibition zone diameters of 15 and 16 mm at a concentration of 60 µg/disk against *E. coli* strain, respectively.<sup>47</sup> However, a slight increase in the zone of inhibition was seen when the concentration of AgNPs was duplicated against the tested strains. These results were consistent with those of a prior study that found that AgNPs had antibacterial activity against the MRSA strain at concentrations of 50 and 100 µg/disk, with zones of inhibition measuring  $15 \pm 1.0$  and  $18 \pm 0.6$  mm, respectively.<sup>48</sup> On the other hand, severe infections brought on by carbapenem-resistant Enterobacterales have been linked to high fatality rates, frequently surpassing 40%.<sup>49</sup> According to a recent publication, between March 2018 and March 2021, 116 strains of carbapenem-resistant *Klebsiella pneumoniae* were isolated from patients hospitalized in adult intensive care units (ICUs), and another 34 strains were isolated from both pediatric and

**Table 2** Screening of Antibacterial Efficacy of Green AgNPs Against the Tested Bacterial Strains

The Tested Strains	Inhibitory Zone Diameters (mm)			-ve Control
	AgNPs (50 µg/Disk)	AgNPs (100 µg/Disk)	Fosfomycin (50µg/Disk)	
<i>E. coli</i>	21.69 ± 0.12	23.18 ± 0.36	23.78 ± 0.12	0.00 ± 0.00
<i>E. cloacae</i>	12.82 ± 0.36	13.97 ± 0.17	20.16 ± 0.41	0.00 ± 0.00
<i>K. pneumoniae</i>	18.35 ± 0.24	20.65 ± 0.51	9.31 ± 0.18	0.00 ± 0.00
MRSA	14.54 ± 0.15	16.29 ± 0.28	24.91 ± 0.27	0.00 ± 0.00

**Notes:** Negative controls referred to filter paper disks impregnated with methanol solvent only.

neonatal ICUs.<sup>50</sup> Interestingly, the antimicrobial potency of the biogenic AgNPs against *K. pneumoniae* ATCC 700603 strain was 2 fold higher than that of fosfomycin antibiotic at a concentration of 50 µg/disk as seen in Table 2.

Methicillin-resistant *Staphylococcus aureus* (MRSA) infections generally result in increased health care expenses, morbidity, prolonged hospitalization time, and decreased quality of life. According to estimates, 170,000 MRSA infections occur annually in European healthcare systems, resulting in over 5000 mortalities, over 1 million extra inpatient days, and additional expenses of over €380 million.<sup>51</sup> Furthermore, *E. cloacae* is responsible for up to 5% of instances of nosocomial pneumonia, 5% of nosocomial sepsis, 4% of nosocomial urinary tract infections, and 10% of postsurgical peritonitis illnesses worldwide.<sup>52</sup> Remarkably, the biogenic AgNPs exposed antimicrobial effectiveness against *E. cloacae* ATCC 13047 and MRSA ATCC 43300, recording suppressive zone diameters of  $13.97 \pm 0.17$  and  $16.29 \pm 0.28$  mm, respectively. The antimicrobial bioactivity data were in agreement with those of Qasim Nasar et al 2019 who indicated that the *Seriphedum quettense* mediated silver nanoparticles (100 µg/mL) demonstrating that *E. coli* strain was the most sensitive strain to the biogenic AgNPs in comparison to the other tested bacterial strains as *B. subtilis*, *S. aureus*, and *K. pneumoniae*.<sup>53</sup>

The minimum inhibitory concentration of AgNPs was tested against the *E. coli* strain, which showed the highest susceptibility to biosynthesized AgNPs. In this regard, the MIC of the biogenic AgNPs against *E. coli* strain was found to be 15 µg/mL, whereas MBC was found to be 20 µg/mL. Interestingly, the detected MIC value of biogenic AgNPs against *E. coli* strain was lower than that detected in a prior report which demonstrated MIC value of 300 µg/mL indicating the high efficiency of synthesis method followed in our current investigation.<sup>54</sup> The biogenic silver nanomaterials utilize several mechanisms of actions, contributing to their potent antibacterial effectiveness. Here are four of AgNPs' documented antibacterial effects: (1) adherence to the microbial membrane's surface, (2) AgNPs disrupt cellular biomolecules after internalization into bacterial cells resulting in intracellular damage, (3) they cause cellular toxicity by producing reactive oxygen species (ROS) that create oxidative stress in the cell, and (4) they interfere with the cell's signal transduction pathways.<sup>55</sup> In this regard, the biogenic AgNPs exposed a higher antibacterial activity against Gram-negative bacterial strains as *E. coli*, and *K. pneumoniae* compared to the tested Gram-positive strain, namely MRSA. The thickness and configuration of the bacterial' cell walls also has an impact on the antibacterial activity of AgNPs. AgNPs are more effective against Gram-negative bacteria like *E. coli* than Gram-positive bacteria like *S. aureus*. This is brought on by variations in how peptidoglycan, a crucial part of the cell membrane, is organized.<sup>56</sup> The negatively charged peptidoglycan layer (30 nm thick) that makes up the cell wall of G+ve bacteria is considerably thicker in these bacteria than in G-ve bacteria (3–4 nm). Accordingly, G+ve bacteria are less vulnerable to AgNPs because their cell walls are comparably thicker than those of G-ve bacteria.<sup>57</sup> A previous study reported that the size of AgNPs is an important factor in determining the antimicrobial activity of biogenic silver nanoparticles, which explains the considerable antibacterial activity of the produced AgNPs measuring 58 nm.<sup>58</sup> The small-sized nanoparticles have a high surface-to-volume ratio, allowing them to engage efficiently with bacterial cells and eventually cause bacterial cell death.

Electrostatic interactions between AgNPs and bacterial cell wall and membranes are reported to cause morphological changes in membrane structure (Figure 11), which in turn disrupts membrane permeability and respiratory functions via membrane depolarization, ultimately leading to disruption of cell integrity and cell death. Accordingly, the disruption of bacterial cell wall and membrane results in the release of its vital contents, such as proteins, enzymes, DNA, ions, metabolites into the surrounding environment.<sup>59</sup>



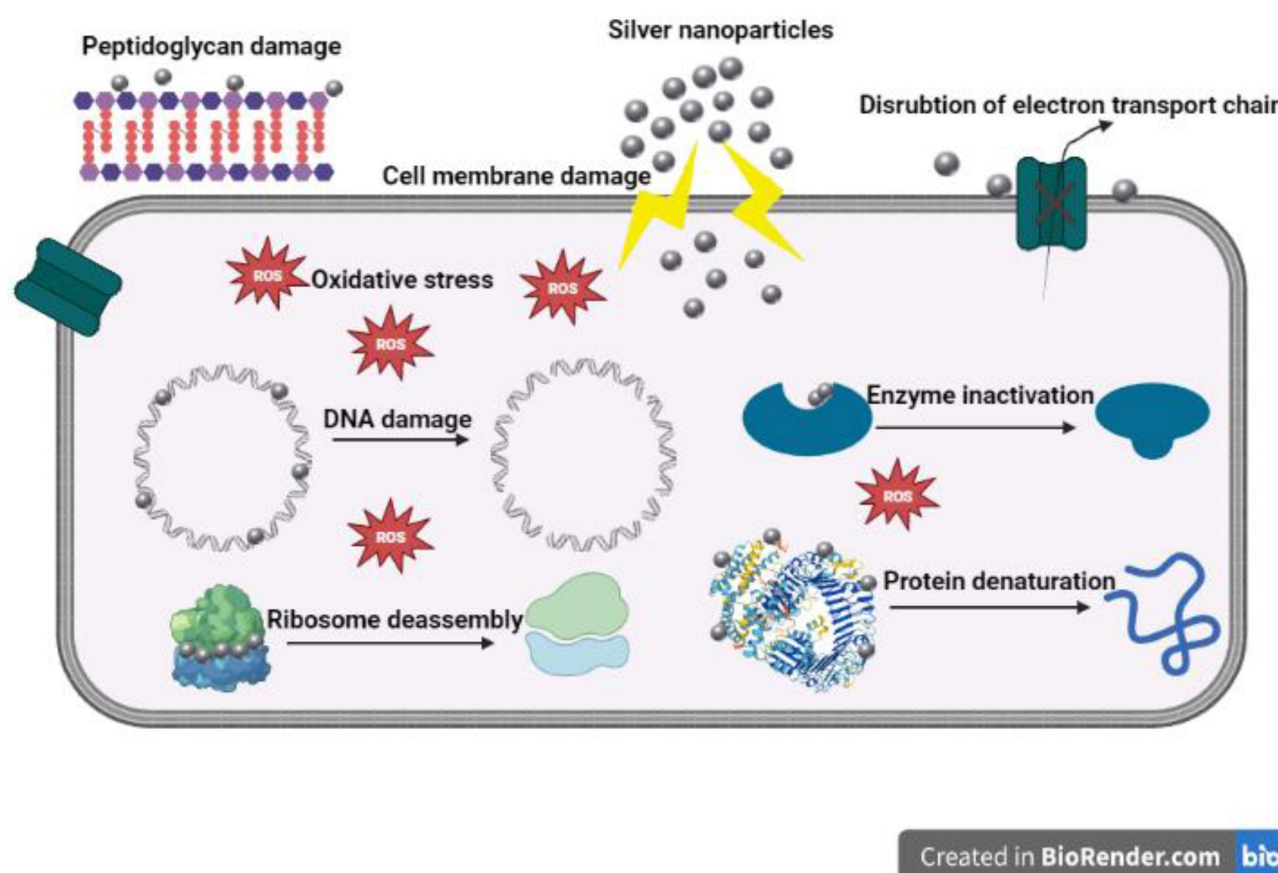


**Figure 11** Proposed antibacterial mechanism of AgNPs against bacterial cells.

## Synergistic Antibacterial Efficiency of Silver Nanoparticles with Fosfomycin Against Different Bacterial Pathogens

The synergistic patterns of the biogenic AgNPs with fosfomycin antibiotic were evaluated using the standardized disk diffusion assay as seen in [Figure 12](#). The highest synergism percent (64.22%) of fosfomycin – AgNPs combination was detected against *K. pneumoniae* strain ATCC 700603, demonstrating suppressive zone of  $27.34 \pm 0.45$  mm compared to  $9.78 \pm 0.11$  mm inhibition zone of fosfomycin antibiotic alone as seen in [Table 3](#). On the other hand, the lowest synergism percentage (3.32%) was detected against *E. cloacae* strain ATCC 13047 recording clear zone of  $22.98 \pm 0.15$  mm in diameter of AgNPs-fosfomycin combination compared to  $22.13 \pm 0.26$  mm of fosfomycin antibiotic only. However, the inhibition zone around fosfomycin disks in *E. cloacae* and MRSA plates showed the presence of pinpoint colonies and this could be attributed to the heteroresistance phenomena which means that the subpopulations of bacterial cells within a bacterial isolate exhibit higher levels of antibiotic resistance in comparison to the susceptible main population.<sup>60</sup> Interestingly, the inhibition zones of AgNPs-fosfomycin disks revealed no presence of these colonies which indicated that the AgNPs boosted the antimicrobial efficiency of fosfomycin antibiotic. In addition, the fosfomycin-AgNPs combination also displayed a moderate synergistic potency against both *E. coli* ATCC 25922 strain recording suppressive zone of  $51.64 \pm 0.25$  mm in diameter with relative synergism percent of 18.35%. Despite the weak and moderate synergistic activity of AgNPs-fosfomycin combination against *E. coli* and MRSA strains, the inhibition zones around fosfomycin disks were significantly higher than those of initial screening test. In this context, the biogenic AgNPs diffused through the medium and boosted the antimicrobial activity of fosfomycin antibiotic against *E. coli* and MRSA strains and this explained the increasing in inhibition zones of fosfomycin antibiotic in synergism test compared to the initial screening test.

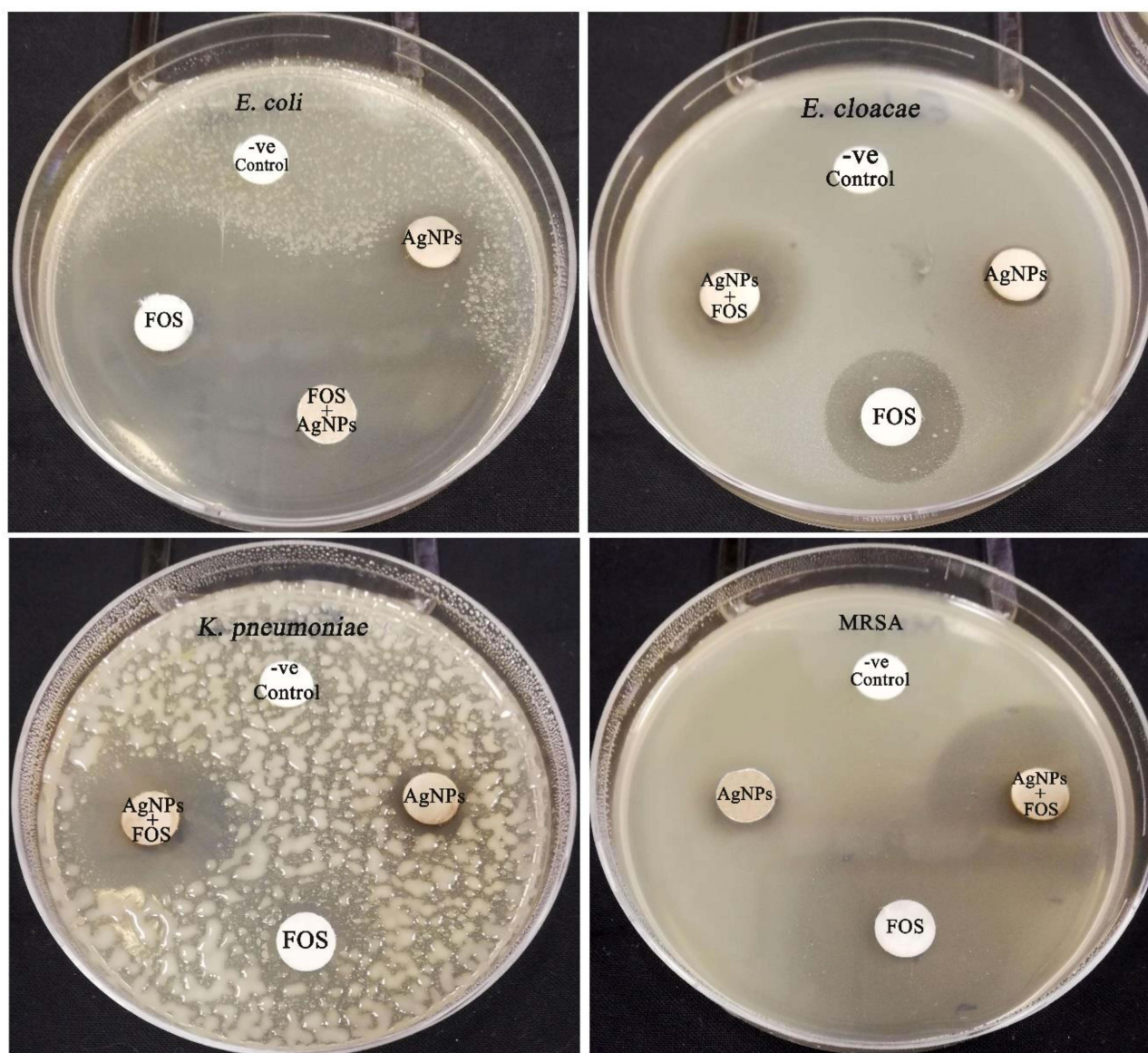


**Figure 12** Antibiogram of the green synthesized AgNPs in combination with fosfomycin antibiotic against different bacterial pathogens.

A previous report confirmed the synergistic antibacterial action of green biofabricated AgNPs utilizing aqueous extract of *Anastatica hierochuntica* with bacitracin, ciprofloxacin, tetracycline, and cefixime antibiotics against *E. coli* strain however antagonistic activity of biogenic AgNPs combined with ciprofloxacin or bacitracin against *S. aureus* strain was observed.<sup>61</sup>

**Table 3** Synergistic Antibacterial Proficiency of Green Silver Nanomaterials with Fosfomycin Antibiotic

The Tested Strains	Inhibition Zone Diameter (mm)			-ve Control	Synergism %
	AgNPs (15 µg/Disk)	Fosfomycin (50 µg/Disk)	Fosfomycin (50 µg/Disk) + AgNPs (15 µg/Disk)		
<i>E. coli</i>	15.46 ± 0.17	42.16 ± 0.38	51.64 ± 0.25	0.00 ± 0.00	18.35%
<i>E. cloacae</i>	10.96 ± 0.34	22.13 ± 0.26	22.98 ± 0.15	0.00 ± 0.00	3.32%
<i>K. pneumoniae</i>	12.78 ± 0.14	9.78 ± 0.11	27.34 ± 0.45	0.00 ± 0.00	64.22%
MRSA	11.56 ± 0.12	35.24 ± 0.45	36.78 ± 0.61	0.00 ± 0.00	4.18%

**Notes:** Negative controls referred to filter paper disks impregnated with methanol solvent only.

The synergistic mode of action might be due to the fact that both of the biofabricated AgNPs and fosfomycin targeted different bacterial cellular constituents. In this regard, the generation of reactive oxygen species (ROS), which result in fatal oxidative damage, is the primary antibacterial mode of action of AgNPs. The ROS such as singlet oxygen ( $O_2$ ), hydrogen peroxide ( $H_2O_2$ ), the superoxide radical ( $O_2^-$ ) and the hydroxyl radical (OH) were generated as a result of microbial aerobic metabolism, which were then neutralized using the antioxidant machinery of microbial cells.<sup>62</sup> However, when ROS generation reaches the threshold that causes the antioxidant machinery in microbial cells to shut down, cellular homeostasis is lost, which leads to the oxidation of essential cellular components including DNA, lipids, and proteins. The AgNPs antibacterial mode of action also involves the oxidation of cellular lipids utilizing ROS resulting in disruption of cell membrane and impairment of its permeability resulting in induction of bacterial cell death.<sup>63</sup>

Fosfomycin is a low-molecular-weight phosphonic acid derivative that was first isolated from *Streptomyces* species.<sup>64</sup> Moreover, the physicochemical profile of fosfomycin, which has a low molecular weight (138 Da) and distinctive hydrophilic qualities along with a negligible affinity for plasma proteins, allows for a wide distribution into a variety of tissues. Furthermore, fosfomycin antibiotic exposed its antibacterial mode of action through interfering with the initial phases of peptidoglycan synthesis and thus disrupting the biosynthesis of bacterial cell walls. In detail, fosfomycin is a phosphoenolpyruvate analogue that inhibits the enzyme enolpyruvate transferase (MurA), which catalyzes the first step in peptidoglycan biosynthesis, and prevents the formation of N-acetylmuramic acid, which is an essential precursor for the peptidoglycan cell wall.<sup>65</sup> Fosfomycin revealed potential antibacterial activity against *E. coli* ATCC 25922 strain however *K. pneumoniae* ATCC 700603 revealed fosfomycin resistance which was mediated by amino acid variations in MurA transporters as reported in prior study.<sup>98</sup> In addition, *E. cloacae* ATCC 13047 and MRSA ATCC 43300 strains revealed heteroresistance to fosfomycin antibiotic which was observed as pinpoint colonies in the inhibition zone around fosfomycin disk. Interestingly, the biogenic AgNPs boosted the antibacterial potency of fosfomycin antibiotic against the targeted bacterial pathogens, determining their maximum synergistic efficiency against *K. pneumoniae* strain ATCC 700603 with synergistic percentage of 64.22%. Collectively, we proposed that the powerful antibacterial action resulted from fosfomycin's disruption of bacterial cell wall synthesis through inhibition of the enzyme enolpyruvate transferase (MurA) and interference with peptidoglycan synthesis, which in turn caused the cell wall to become weaker and facilitate the internalization of AgNPs, which act by producing ROS and oxidizing various cellular components, such as DNA, protein, and lipids.

## Conclusions

The flower extract of *H. sabdariffa* facilitated green biofabrication of AgNPs with potential physicochemical features and a remarkable antibacterial bioactivity against the targeted nosocomial bacterial pathogens. The potential antimicrobial effectiveness of the biosynthesized AgNPs against the tested strains emphasizes the potential application of these nanoparticles for the control of nosocomial and drug-resistant pathogens in health care facilities and intensive care units. The AgNPs-fosfomycin combination showed a high potency against the tested strains so that this combination could be a promising source of effective antibacterial agents contributing for the successful management of nosocomial bacterial pathogens in hospitals and health care settings.

## Acknowledgment

The authors extend their appreciation to the Deanship of Scientific Research, King Saud University for funding through Vice Deanship of Scientific Research Chairs, Research Chair of Medical and Molecular Genetics.

## Disclosure

The authors report no conflicts of interest in this work.

## References

1. Murray CJ, Ikuta KS, Sharara F, et al. Global burden of bacterial antimicrobial resistance in 2019: a systematic analysis. *Lancet*. 2022;399:629–655. doi:10.1016/S0140-6736(21)02724-0
2. Owolabi JB, Olatunde SKA. Review of prevalence, antimicrobial susceptibility patterns and molecular characteristics of methicillin-resistant staphylococcus aureus (mrsa) in the Caribbean. *Adv Microbiol*. 2022;12:459–480. doi:10.4236/aim.2022.128032



3. Vivas R, Barbosa AAT, Dolabela SS, Jain S. Multidrug-resistant bacteria and alternative methods to control them: an overview. *Microb Drug Resist.* 2019;25:890–908. doi:10.1089/mdr.2018.0319
4. Roy A, Bulut O, Some S, Mandal AK, Yilmaz MD. green synthesis of silver nanoparticles: biomolecule-nanoparticle organizations targeting antimicrobial activity. *RSC Adv.* 2019;9:2673–2702. doi:10.1039/C8RA08982E
5. Tripathi N, Goshisht MK. Recent advances and mechanistic insights into antibacterial activity, antibiofilm activity, and cytotoxicity of silver nanoparticles. *ACS Appl Bio Mater.* 2022;5(4):1391–1463. doi:10.1021/acsabm.2c00014
6. Prabhu S, Poulse EK. Silver nanoparticles: mechanism of antimicrobial action, synthesis, medical applications, and toxicity effects. *Int Nano Lett.* 2012;2:1–10. doi:10.1186/2228-5326-2-32
7. Jeevanandam J, Kiew SF, Boakye-Ansah S, et al. Green approaches for the synthesis of metal and metal oxide nanoparticles using microbial and plant extracts. *Nanoscale.* 2022;14:2534–2571. doi:10.1039/D1NR08144F
8. Ijaz M, Zafar M, Iqbal T. Green synthesis of silver nanoparticles by using various extracts: a review. *Inorg Nano-Met Chem.* 2020;51:744–755. doi:10.1080/24701556.2020.1808680
9. Salem MA, Zayed A, Beshay ME, et al. *Hibiscus sabdariffa* L.: phytoconstituents, nutritive, and pharmacological applications. *Adv Trad Med.* 2022;22(3):497–507. doi:10.1007/s13596-020-00542-7
10. Arslan M, Zareef M, Tahir HE, Rakha A, Xiaobo Z, Mahunu GK. Medicinal and therapeutic potential of roselle (*Hibiscus sabdariffa*). In: *Roselle (Hibiscus Sabdariffa)*. Amsterdam, The Netherlands: Elsevier; 2021:155–186.
11. Guan Q, Xia C, Li W. Bio-friendly controllable synthesis of silver nanoparticles and their enhanced antibacterial property. *Catal Today.* 2019;327:196–202. doi:10.1016/j.cattod.2018.05.004
12. Bao Y, He J, Song K, Guo J, Zhou X, Liu S. Plant-extract-mediated synthesis of metal nanoparticles. *J Chem.* 2021;2021:6562687.
13. Salayová A, Bedlovičová Z, Daneu N, et al. Green synthesis of silver nanoparticles with antibacterial activity using various medicinal plant extracts: morphology and antibacterial efficacy. *Nanomaterials.* 2021;11:1005. doi:10.3390/nano11041005
14. Khane Y, Benouis K, Albukhaty S, et al. Green synthesis of silver nanoparticles using aqueous citrus limon zest extract: characterization and evaluation of their antioxidant and antimicrobial properties. *Nanomaterials.* 2022;12:2013. doi:10.3390/nano12122013
15. Mubeen B, Ansar AN, Rasool R, et al. Nanotechnology as a novel approach in combating microbes providing an alternative to antibiotics. *Antibiotics.* 2021;10:1473. doi:10.3390/antibiotics10121473
16. Rawat V, Sharma A, Bhatt VP, Singh RP, Maurya IK. Sunlight mediated green synthesis of silver nanoparticles Using *Polygonatum Graminifolium* leaf extract and their antibacterial activity. *Mater Today Proc.* 2020;29:911–916. doi:10.1016/j.matpr.2020.05.274
17. Abdelsattar AS, Hakim TA, Rezk N, et al. Green synthesis of silver nanoparticles using *Ocimum basilicum* L. and *Hibiscus sabdariffa* L. extracts and their antibacterial activity in combination with phage zcse6 and sensing properties. *J Inorg Organomet Polym Mater.* 2022;2022:1–15.
18. Khan MR, Hoque SM, Hossain KFB, Siddique MAB, Uddin MK, Rahman MM. Green synthesis of silver nanoparticles using *Hibiscus sabdariffa* leaf extract and its cytotoxicity assay. *Inorg Nano Met Chem.* 2022;2022:1–11.
19. Yassin MT, Mostafa AA-F, Al-Askar AA, Alkhelaif AS. In vitro antimicrobial potency of *Elettaria Cardamomum* ethanolic extract against multidrug resistant of food poisoning bacterial strains. *J King Saud Univ Sci.* 2022;34:102167. doi:10.1016/j.jksus.2022.102167
20. Pourjavadi A, Soleyman R. Silver nanoparticles with gelatin nanoshells: photochemical facile green synthesis and their antimicrobial activity. *J Nanoparticle Res.* 2011;13:4647–4658. doi:10.1007/s11051-011-0428-6
21. Yassin MT, Mostafa AA-F, Al-Askar AA, Al-Otibi FO. Facile green synthesis of zinc oxide nanoparticles with potential synergistic activity with common antifungal agents against multidrug-resistant candidal strains. *Crystals.* 2022;12:774. doi:10.3390/cryst12060774
22. Clinical and Laboratory Standards. *Performance Standards for Antimicrobial Disk Susceptibility Tests; Approved Standard M2-A8*. Wayne, PA, USA: Clinical and Laboratory Standards Institute (CLSI); 2003.
23. Vanti GL, Nargund VB, Vanarchi R, et al. Synthesis of *Gossypium hirsutum*-derived silver nanoparticles and their antibacterial efficacy against plant pathogens. *Appl Organomet Chem.* 2019;33(1):e4630. doi:10.1002/aoc.4630
24. Njume C, Afolayan AJ, Green E, Ndip RN. Volatile compounds in the stem bark of *Sclerocarya birrea* (Anacardiaceae) possess antimicrobial activity against drug-resistant strains of *Helicobacter Pylori*. *Int J Antimicrob Agents.* 2011;38:319–324. doi:10.1016/j.ijantimicag.2011.05.002
25. Moteriya P, Padalia H, Chanda S. Characterization, synergistic antibacterial and free radical scavenging efficacy of silver nanoparticles synthesized using *Cassia roxburghii* leaf extract. *J Genet Eng Biotechnol.* 2017;15(2):505–513. doi:10.1016/j.jgeb.2017.06.010
26. Roy P, Das B, Mohanty A, Mohapatra S. Green synthesis of silver nanoparticles using *Azadirachta Indica* leaf extract and its antimicrobial study. *Appl Nanosci.* 2017;7:843–850. doi:10.1007/s13204-017-0621-8
27. Rupiasih NN, Aher A, Gosavi S, Vidyasagar PB. *Green Synthesis of Silver Nanoparticles Using Latex Extract of Thevetia Peruviana: A Novel Approach Towards Poisonous Plant Utilization, in Recent Trends in Physics of Material Science and Technology*. Springer; 2015:1–10.
28. Fatimah I, Afrid ZHVI. Characteristics and antibacterial activity of green synthesized silver nanoparticles using red spinach (*Amaranthus Tricolor* L.) leaf extract. *Green Chem Lett Rev.* 2019;12:25–30. doi:10.1080/17518253.2019.1569729
29. Philip D. Green synthesis of gold and silver nanoparticles using *hibiscus rosa sinensis*. *Phys E Low Dimens Syst Nanostructures.* 2010;42:1417–1424. doi:10.1016/j.physe.2009.11.081
30. Shivaji S, Madhu S, Singh S. Extracellular synthesis of antibacterial silver nanoparticles using psychrophilic bacteria. *Process Biochem.* 2011;46(9):1800–1807. doi:10.1016/j.procbio.2011.06.008
31. Subbaiya R, Saravanan M, Priya AR, et al. Biomimetic synthesis of silver nanoparticles from *Streptomyces Atrovirens* and their potential anticancer activity against human breast cancer cells. *IET Nanobiotechnol.* 2017;11:965–972. doi:10.1049/iet-nbt.2016.0222
32. Iftekhar S, Nazir F, Abbasi NM, Khan AA, Ahmed F. *Rumex Hastatus* mediated green synthesis of agnps: an efficient nanocatalyst and colorimetric probe for Cu<sup>2+</sup>. *Colloids Surf Physicochem Eng Asp.* 2021;628:127356. doi:10.1016/j.colsurfa.2021.127356
33. Dhar SA, Chowdhury RA, Das S, Nahian MK, Islam D, Gafur MA. Plant-mediated green synthesis and characterization of silver nanoparticles using *Phyllanthus Emblica* fruit extract. *Mater Today Proc.* 2021;42:1867–1871. doi:10.1016/j.matpr.2020.12.222
34. Yassin MT, Mostafa AA-F, Al-Askar AA, Al-Otibi FO. Synergistic antibacterial activity of green synthesized silver nanomaterials with colistin antibiotic against multidrug-resistant bacterial pathogens. *Crystals.* 2022;12:1057. doi:10.3390/cryst12081057
35. Sidorowicz A, Szymański T, Rybka JD. Photodegradation of biohazardous dye brilliant blue r using organometallic silver nanoparticles synthesized through a green chemistry method. *Biology.* 2021;10:784. doi:10.3390/biology10080784



36. Das G, Patra JK, Debnath T, Ansari A, Shin H-S. Investigation of antioxidant, antibacterial, antidiabetic, and cytotoxicity potential of silver nanoparticles synthesized using the outer peel extract of *Ananas Comosus* (L.). *PLoS One*. 2019;14:e0220950. doi:10.1371/journal.pone.0220950
37. Govindan L, Anbazhagan S, Altemimi AB, et al. Efficacy of antimicrobial and larvicidal activities of green synthesized silver nanoparticles using leaf extract of *Plumbago Auriculata* Lam. *Plants*. 2020;9:1577. doi:10.3390/plants9111577
38. Sinha SN, Paul D, Halder N, Sengupta D, Patra SK. Green synthesis of silver nanoparticles using fresh water green alga *Pithophora Oedogonia* (Mont.) Wittrock and evaluation of their antibacterial activity. *Appl Nanosci*. 2015;5:703–709. doi:10.1007/s13204-014-0366-6
39. Renganathan S, Subramaniyan S, Karunanithi N, et al. antibacterial, antifungal, and antioxidant activities of silver nanoparticles biosynthesized from *Bauhinia Tomentosa* Linn. *Antioxidants*. 2021;10:1959. doi:10.3390/antiox10121959
40. Nayak D, Ashe S, Rauta PR, Kumari M, Nayak B. bark extract mediated green synthesis of silver nanoparticles: evaluation of antimicrobial activity and antiproliferative response against osteosarcoma. *Mater Sci Eng C*. 2016;58:44–52. doi:10.1016/j.msec.2015.08.022
41. Sadeghi B, Rostami A, Momeni SS. Facile green synthesis of silver nanoparticles using seed aqueous extract of *Pistacia Atlantica* and its antibacterial activity. *Spectrochim Acta A Mol Biomol Spectrosc*. 2015;134:326–332. doi:10.1016/j.saa.2014.05.078
42. Mudalige T, Qu H, Van Haute D, Ansar SM, Paredes A, Ingle T. Characterization of nanomaterials: tools and challenges. *Nanomater Food Appl*. 2019;2019:313–353.
43. Jamil K, Khattak SH, Farrukh A, et al. Biogenic synthesis of silver nanoparticles using *Catharanthus Roseus* and its cytotoxicity effect on vero cell lines. *Molecules*. 2022;27:6191. doi:10.3390/molecules27196191
44. Mukherjee S, Sau S, Madhuri D, et al. green synthesis and characterization of monodispersed gold nanoparticles: toxicity study, delivery of doxorubicin and its bio-distribution in mouse model. *J Biomed Nanotechnol*. 2016;12:165–181. doi:10.1166/jbn.2016.2141
45. Cullen IM, Manecksha RP, McCullagh E, et al. The changing pattern of antimicrobial resistance within 42 033 *Escherichia Coli* Isolates from nosocomial, community and urology patient-specific urinary tract infections, Dublin, 1999–2009. *BJU Int*. 2012;109:1198–1206. doi:10.1111/j.1464-410X.2011.10528.x
46. Orole OO, Gambo SM, Fadayomi VS. Characteristics of virulence factors and prevalence of virulence markers in resistant *Escherichia coli* from patients with gut and urinary infections in Lafia, nigeria. *Microbiol Insights*. 2022;15:11786361221106992. doi:10.1177/11786361221106993
47. Hossain MM, Polash SA, Takikawa M, et al. Investigation of the antibacterial activity and in vivo cytotoxicity of biogenic silver nanoparticles as potent therapeutics. *Front Bioeng Biotechnol*. 2019;7:239. doi:10.3389/fbioe.2019.00239
48. Vijayakumar S, Malaikozhundan B, Parthasarathy A, Saravanakumar K, Wang MH, Vaseeharan B. Nano biomedical potential of biopolymer chitosan-capped silver nanoparticles with special reference to antibacterial, antibiofilm, anticoagulant and wound dressing material. *J Cluster Sci*. 2020;31(2):355–366. doi:10.1007/s10876-019-01649-x
49. Tzouveleakis LS, Markogiannakis A, Psychogiou M, Tassios PT, Daikos GL. Carbapenemases in *Klebsiella pneumoniae* and other Enterobacteriaceae: an evolving crisis of global dimensions. *Clin Microbiol Rev*. 2012;25:682–707. doi:10.1128/CMR.05035-11
50. Zarras C, Pappa S, Zarras K, et al. Changes in molecular epidemiology of carbapenem-resistant *Klebsiella pneumoniae* in the intensive care units of a Greek hospital, 2018–2021. *Acta Microbiol Immunol Hung*. 2022;2022:1.
51. Salmanov AG, Verner OM. Prevalence of Methicillin-Resistant *Staphylococcus Aureus* (MRSA) in Kyiv Surgical Hospital (Ukraine). *Int J Antibiotics Probiotics*. 2017;1:73–83. doi:10.31405/ijap.1-2.17.05
52. Mezzatesta ML, Gona F, Stefani S. Enterobacter cloacae complex: clinical impact and emerging antibiotic resistance. *Future Microbiol*. 2012;7:887–902. doi:10.2217/fmb.12.61
53. Qasim Nasar M, Zohra R, Khalil AT, et al. *Seripheidium Quettense* mediated green synthesis of biogenic silver nanoparticles and their theranostic applications. *Green Chem Lett Rev*. 2019;12:310–322. doi:10.1080/17518253.2019.1643929
54. Liu P, Zhao WH, Song YP, et al. Characterization, antimicrobial, and antioxidant potentialities of first-time isolated silver nanoparticles synthesizing protein secreted by *Lysinibacillus sphaericus*. *Process Biochem*. 2022;122:230–237. doi:10.1016/j.procbio.2022.08.032
55. Dakal TC, Kumar A, Majumdar RS, Yadav V. Mechanistic basis of antimicrobial actions of silver nanoparticles. *Front Microbiol*. 2016;7:1831. doi:10.3389/fmicb.2016.01831
56. Arsène MM, Podoprigora IV, Davares AK, Razan M, Das MS, Senyagin AN. Antibacterial activity of grapefruit peel extracts and green-synthesized silver nanoparticles. *Vet World*. 2021;14:1330. doi:10.14202/vetworld.2021.1330-1341
57. Rai M, Kon K, Ingle A, Duran N, Galdiero S, Galdiero M. Broad-spectrum bioactivities of silver nanoparticles: the emerging trends and future prospects. *Appl Microbiol Biotechnol*. 2014;98:1951–1961. doi:10.1007/s00253-013-5473-x
58. Tang S, Zheng J. Antibacterial activity of silver nanoparticles: structural effects. *Adv Health Care Mater*. 2018;7(13):e1701503. doi:10.1002/adhm.201701503
59. Slavin YN, Asnis J, Häfeli UO, Bach H. Metal nanoparticles: understanding the mechanisms behind antibacterial activity. *J Nanobiotechnol*. 2017;15(1):1–20. doi:10.1186/s12951-017-0308-z
60. El-Halfawy OM, Valvano MA. Antimicrobial heteroresistance: an emerging field in need of clarity. *Clin Microbiol Rev*. 2015;28(1):191–207. doi:10.1128/CMR.00058-14
61. Aabed K, Mohammed AE. Synergistic and antagonistic effects of biogenic silver nanoparticles in combination with antibiotics against some pathogenic microbes. *Front Bioeng Biotechnol*. 2021;9:652362. doi:10.3389/fbioe.2021.652362
62. Hengyi XU, Qu F, Xu H, et al. Role of reactive oxygen species in the antibacterial mechanism of silver nanoparticles on *Escherichia coli* O157: H7. *Biomaterials*. 2012;25(1):45–53. doi:10.1007/s10534-011-9482-x
63. Gkartzou F, Giormezis N, Spiliopoulou I, Antimisiaris SG. Nanobiosystems for antimicrobial drug-resistant infections. *Nanomaterials*. 2021;11:1075. doi:10.3390/nano11051075
64. Dos Santos C, Dos Santos LS, Franco OL. Fosfomycin and nitrofurantoin: classic antibiotics and perspectives. *J Antibiot*. 2021;74:547–558. doi:10.1038/s41429-021-00444-z
65. Gil-Gil T, Ochoa-Sánchez LE, Martínez JL. The antibiotic fosfomycin mimics the effects of the intermediate metabolites phosphoenolpyruvate and glyceraldehyde-3-phosphate on the *Stenotrophomonas maltophilia* transcriptome. *Int J Mol Sci*. 2021;23:159. doi:10.3390/ijms23010159

**Infection and Drug Resistance****Dovepress****Publish your work in this journal**

Infection and Drug Resistance is an international, peer-reviewed open-access journal that focuses on the optimal treatment of infection (bacterial, fungal and viral) and the development and institution of preventive strategies to minimize the development and spread of resistance. The journal is specifically concerned with the epidemiology of antibiotic resistance and the mechanisms of resistance development and diffusion in both hospitals and the community. The manuscript management system is completely online and includes a very quick and fair peer-review system, which is all easy to use. Visit <http://www.dovepress.com/testimonials.php> to read real quotes from published authors.

Submit your manuscript here: <https://www.dovepress.com/infection-and-drug-resistance-journal>